

Corrosion behavior of Eurofer 97 and ODS-Eurofer alloys compared to traditional stainless steels

Maysa Terada · Angelo José de Oliveira Zimmermann ·

Hugo Ricardo Zschommler Sandim ·

Isolda Costa · Angelo Fernando Padilha

Received: 13 May 2010/Accepted: 15 May 2011/Published online: 29 May 2011

© Springer Science+Business Media B.V. 2011

Abstract In the present work, the corrosion resistance of ferritic-martensitic EUROFER 97 and ODS-EUROFER steels was tested in solutions containing NaCl or H₂SO₄ and KSCN, both at 25 °C. The results were compared to those of AISI 430 ferritic and AISI 410 martensitic conventional stainless steels. The as-received samples were tested by electrochemical techniques, specifically, electrochemical impedance spectroscopy, potentiodynamic polarization curves, and double-loop electrochemical potentiokinetic reactivation tests. The surfaces were observed by scanning electron microscopy after exposure to corrosive media. The results showed that EUROFER 97 and ODS-EUROFER alloys present similar corrosion resistance but lower than ferritic AISI 430 and martensitic 410 stainless steels.

Keywords Eurofer 97 · ODS-Eurofer · Corrosion · DL-EPR tests · EIS

M. Terada (✉)

Laboratório de Microscopia, Laboratório Nacional de Luz Síncrotron, Rua Giuseppe Máximo Scolfaro, 10.000 Pólo II de Alta Tecnologia, Campinas
e-mail: maysaterada@uol.com.br

A. J. de Oliveira Zimmermann · A. F. Padilha

Departamento de Engenharia Metalúrgica e de Materiais, Escola Politécnica da Universidade de São Paulo, Av. Prof. Mello de Moraes, 2463, CEP 05508-030 São Paulo, SP, Brazil

H. R. Z. Sandim

Departamento de Engenharia de Materiais, Escola de Engenharia de Lorena, Polo Urbo-Industrial, Universidade de São Paulo, Gleba Al-6, Lorena, SP, Brazil

I. Costa

Instituto de Pesquisas Energéticas e Nucleares-CCTM, Av. Prof. Lineu Prestes, 2242, CEP 05508-900 São Paulo, SP, Brazil

1 Introduction

Ferritic-martensitic steels show reasonably good thermo-physical and mechanical properties, low sensitivity to radiation-induced swelling and helium embrittlement under (fission) neutron irradiation and good compatibility with major cooling and breeding materials. In recent years, reduced-activation versions of this type of steels have been developed in Japan and Europe in laboratory scale and tested with equivalent or even better mechanical properties. Reduced-activation-ferritic-martensitic (RAFM) steels are considered for application in fusion technology as structural materials for the first wall of future fusion reactors DEMO [1].

Eurofer 97 alloy is a new RAFM steel developed on the basis of the experience gained with OPTIFER, MANET and F82H-modified type steels to replace conventional Cr-Mo steels in structural components for fusion reactors. Its chemical composition has been designed and optimized to obtain fairly good thermo-physical and mechanical properties, low sensitivity to radiation-induced swelling and helium embrittlement under (fission) neutron irradiation and good compatibility with major cooling and breeding materials when compared to other fusion structural materials [2–4].

Oxide dispersion strengthened (ODS) alloys have been developed to increase the working temperature of RAFM steels increasing their potentiality for applications in fusion reactors that operate at temperatures higher than 650 °C. A first generation of ODS alloys was developed and has been produced in cooperation with Plansee AG (Austria). The microstructure and mechanical properties of these alloys has already been studied [3, 5–20].

According to literature [3–5, 21–27], the main carbide formed in Eurofer alloys is M₂₃C₆, but smaller quantities of

nitrides, other carbides and carbonitrides may also be found [9, 13, 21]. $M_{23}C_6$ carbides [3] are responsible for lower ductility and impact resistance [22, 23] and higher sensitization process. However, there are only a few papers that considered the corrosion resistance of Eurofer alloys in liquid metals [24–29] and in pure water [30, 31], but none of them took into account intergranular corrosion caused by precipitates.

Intergranular corrosion in stainless steels has been known and investigated for nearly 100 years [32–34]. A literature search on stainless steels using the keywords *intergranular corrosion* or *sensitization* reveals that there are thousands of published works on this subject. Nearly 99% of these publications deal with intergranular corrosion in austenitic stainless steels due to chromium depletion at the grain boundaries neighborhood caused by chromium carbide ($M_{23}C_6$) precipitation [35, 36].

The aim of this work is to evaluate the corrosion resistance of RAFM EUROFER 97 and ODS-EUROFER alloys in a 0.1 NaCl mol L⁻¹ solution and their intergranular corrosion resistance in a solution with H₂SO₄ and KSCN at 25 °C, and compare the results with ferritic AISI 430 and martensitic AISI 410 conventional stainless steels. All materials were studied in as-received condition.

2 Experimental

Samples of both Eurofer 97 and RAFM ODS-Eurofer (9Cr-1 W-0.3Y₂O₃) alloys were provided by Forschungszentrum Karlsruhe (FZK). The Eurofer alloy was produced by vacuum arc remelting process (VAR). The ODS-Eurofer alloy was processed by a powder metallurgy route, including inert gas atomization followed by addition of Y₂O₃ particles via high energy milling (mechanical alloying) followed by hot isostatic pressing. Table 1 presents the chemical composition of all materials studied in this work. Both alloys were tested in as-tempered condition. The samples of both AISI 410 and 430 stainless steels were taken from hot extruded bars supplied by Villares Metals.

For corrosion resistance evaluation, the surfaces of all samples were prepared by grinding with SiC paper #4,000.

The specimens were then immersed in a 0.1 NaCl mol L⁻¹ solution at 25 °C, and after 3 h of immersion, electrochemical impedance spectroscopy (EIS) and then anodic potentiodynamic polarization tests were carried out using a Gamry model EIS 300® frequency response analyzer coupled to a Gamry PCI 4/300 potentiostat. All EIS measurements were obtained in the potentiostatic mode at the stabilized open circuit potential. The amplitude of the sinusoidal signal was 10 mV (rms) and the investigated frequency was from 100 kHz to 10 mHz, with an acquisition rate of 10 points per decade. After the EIS tests, potentiodynamic polarization measurements were obtained in the range from the open circuit potential (OCP) up to 10 mA/cm², at a scan rate of 1 mVs⁻¹.

Double-loop electrochemical potentiokinetic reactivation (DL-EPR) method was also performed in a 2 M H₂SO₄ + 0.005 M KSCN solution, at 25 °C, after 5 min of immersion, to quantitatively evaluate the intergranular corrosion resistance of the materials. This solution was developed from the standard ASTM A262 [37]. A three-electrode set-up cell was used, with a saturated calomel electrode (SCE) as reference electrode, a platinum wire as counter electrode and the specimen as working electrode. All the potentials in this work are referred to the SCE electrode. Potentiodynamic polarization tests were carried out from the open circuit potential (OCP) up to 1.0 V_{SCE} at a scan rate of 1 mV s⁻¹. In DL-EPR method, the specimens were anodically polarized from the OCP up to 0.4 V_{SCE} at a scan rate of 1.67 mV s⁻¹. At 0.4 V_{SCE}, the polarization direction was reversed and the test was finished at the initially measured OCP. The samples surface exposed to DL-EPR tests were observed by scanning electron microscopy (SEM) in the secondary electrons mode using a Philips XL30 microscope. The chemical composition of some precipitates was also analyzed using a Philips field emission gun scanning electron microscope.

3 Results and discussion

The microstructures of both Eurofer 97 and ODS-Eurofer alloys were observed using SEM (Fig. 1) after 5 min of

Table 1 Chemical composition of RAFM Eurofer 97 and ODS-Eurofer alloys, martensitic AISI 410 and ferritic AISI 430 stainless steels (wt%)

	Cr	W	Ta	V	C	Mn	Ni	Mo	Y	Fe
ODS-Eurofer (F/M)	8.92	1.110	0.081	0.193	0.071	0.408	0.051	0.004	0.192	Balance
Eurofer 97(F/M)	9.08	1.070	0.125	0.235	0.105	0.560	0.013	—	—	Balance
AISI 410 (M)	12.14	0.013	—	0.030	0.108	0.324	0.312	0.031	—	Balance
AISI 430(F)	16.89	0.013	—	0.042	0.028	0.427	0.360	0.214	—	Balance

F/M ferritic/martensitic; F ferritic; M martensitic

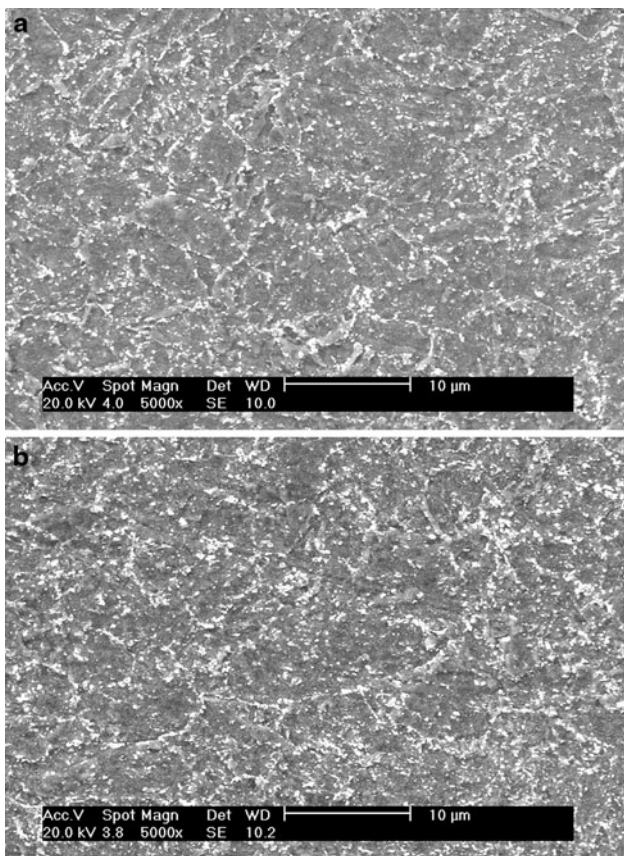


Fig. 1 Scanning electron microscopy micrographs of **a** Eurofer 97 and **b** ODS-Eurofer alloy. Samples were etched in Nital 10% for 5 min

immersion in a solution of Nital 10%. The micrographs show not only the higher amount of precipitates in ODS-Eurofer steel but also its smaller grain size in comparison with Eurofer 97.

The EIS results are shown in Fig. 2. The EIS diagrams showed a very similar shape, corresponding to depressed capacitive arcs for all the studied materials, suggesting analogous electrochemical behavior for all samples. However, the AISI 410 and 430 presented higher impedance values than the Eurofer alloys, suggesting slower charge transfer process associated to the first, likely due to their larger amounts of Cr when compared with the Eurofer alloys. The Bode phase angle diagrams showed a phase angle peak at frequencies between 10 and 1 Hz and a shoulder was indicated for the stainless steels (AISI 410 and 430), at lower frequencies. Surprisingly, the ODS-Eurofer alloy presented lower impedances when compared to the Eurofer 97 alloy, suggesting that Y_2O_3 addition to Eurofer alloy did not change its corrosion resistance.

The EIS data obtained were fitted using the electrical equivalent circuit shown in Fig. 3 where the R_1 -CPE₁ pair corresponds to the high frequency results and is associated

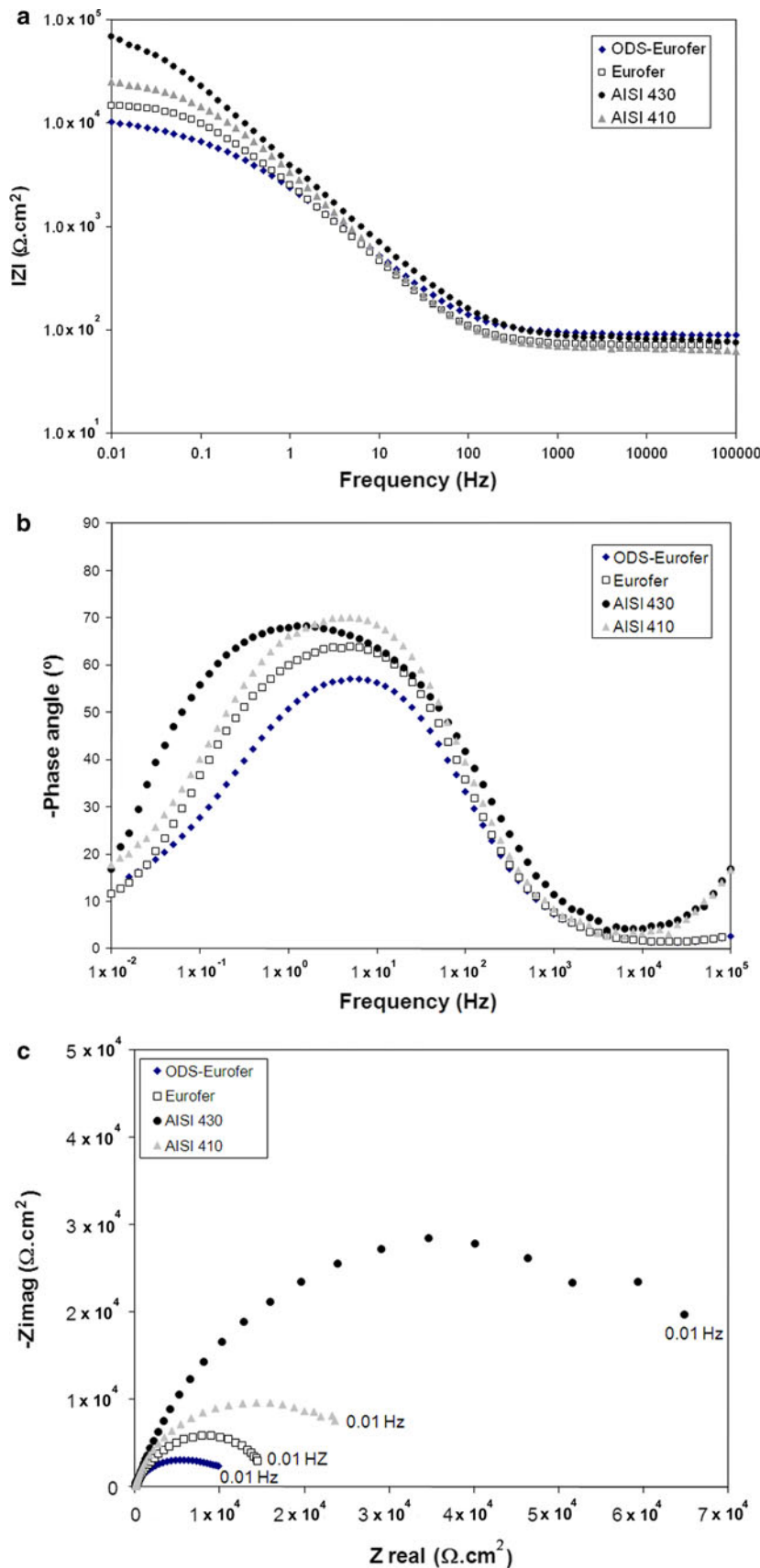
to the oxide film, whereas the R_2 -CPE₂ pair corresponding to the low frequency data is related to interfacial processes and the charging of the double layer. In all cases, the agreement between experimental and fitted data was very good. Table 2 presents the resistance, the CPE and CPE exponent values obtained for the equivalent circuit components in the fitting procedure. The CPE exponents associated to the R_1 -CPE₁ pair (n_1) were around 0.8 for most tested materials, with the exception of the Eurofer alloy, that presented n_1 close to 0.6, indicating the influence of diffusion processes through its oxide layer. For ODS Eurofer alloy and AISI 410 SS, the CPE exponents associated to the interfacial processes (n_2), close to 0.5, indicate diffusion controlled processes, likely due to the defects in their oxide film. The lowest “ n_2 ” value estimated for the ODS-Eurofer alloy suggests a highly heterogeneous oxide. The large amount of precipitates in the ODS-Eurofer alloy, as Fig. 1 shows, and the large C content in the AISI 410 SS (0.105 wt%) associated with very low amount of stabilizers (W and V) could be the reason of these results.

The lowest R_2 and highest CPE₂ values associated to the ODS-Eurofer in the 0.1 NaCl mol L⁻¹ electrolyte, comparatively to the other alloys studied, indicates that it is the one with the lowest corrosion resistance among the investigated materials. These results demonstrate that the addition of Y_2O_3 to the Eurofer alloy, with Cr content of nearly 9 wt%, does not increase its corrosion resistance. In fact, the lower corrosion resistance of the ODS-Eurofer comparatively to the Eurofer 97 can be related to the larger amount of precipitates in the first alloy, in comparison with the second one (Fig. 1). The precipitates seem to be preferentially located at the grain boundaries of both Eurofer alloys, what might lead to decreased intergranular corrosion resistance, as it will be shown afterward.

Potentiodynamic polarization curves (Fig. 4) show that all samples presented an active–passive transition, but the current densities in the passive range were much lower for the ferritic AISI 430 SS (order of 10^{-6} A.cm⁻²), indicating the formation of a more protective film on this SS comparatively to the others. In fact, the current densities at the passive region of the ODS-Eurofer samples were in the order of 10^{-5} A.cm⁻², suggesting that the surface film formed on these samples is not very protective and partial dissolution of metallic material occurs through this film.

The potentiodynamic polarization curves show breakdown potentials around 0.0 V_{SCE} for the AISI 410 and 430 SS and the micrographs of their surfaces after polarization tests (Fig. 5) confirmed the localized corrosion with similar number of pits on their surfaces. However, the pits associated to the AISI 430 (Fig. 5a) were shallower than those on the AISI 410 (Fig. 5b). The surface of these steels suggests not only localized but also generalized attack, Fig. 5c, d. The polarization curves of the ODS-Eurofer

Fig. 2 EIS diagrams **a** Z Modulus, **b** Bode phase and **c** Nyquist obtained after 3 h of immersion in 0.1 NaCl mol L⁻¹ solution at 25 °C



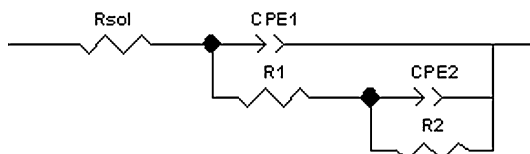


Fig. 3 Equivalent electric circuit for fitting EIS data obtained for all samples immersed in a 0.1 NaCl mol L⁻¹ solution at 25 °C

showed a large increase with applied potential showing that the passive film was easily attacked in the test solution adopted. A larger number of deeper pits were found on this steel comparatively to the Eurofer 97 surface. The generalized attack could be explained by the large amount of M₂₃C₆ randomly distributed in RAFM Eurofer 97 alloy, as reported in the literature [3]. It is plausible that corrosion on these alloys occurs in the vicinity of the M₂₃C₆ particles located inside the grains and also at the grain boundaries, as Fernández et al. [3] proved that Eurofer 97 alloy presents a fine structure with grain size in the range 10–12 µm and Eiselt et al. [4] verified that RAFM ODS-Eurofer alloy exhibits equiaxed grains with sizes between 2 and 8 µm.

According to the polarization curves presented, the ferritic AISI 430 stainless steel showed the highest corrosion resistance and the ODS-Eurofer alloy, the lowest one, among the tested materials. In order to quantitatively evaluate the intergranular corrosion resistance of the samples at the various conditions tested, the double-loop electrochemical potentiokinetic reactivation technique (DL-EPR) was carried out.

The DL-EPR method is based on the passivation followed by reactivation of the stainless steel surface from the passive state. The maximum anodic current (i_a) is obtained from the polarization curves corresponding to the scan in the anodic direction. At 0.4 V_{SCE}, the polarization direction was reversed, and when reactivation of the surface occurs, the maximum current obtained during the reverse scan corresponds to the reactivation current (i_r). For sensitized steels, reactivation occurs preferentially at the grain boundaries and the ratio (i_r/i_a) indicates the steel susceptibility to intergranular corrosion. Table 3 shows the i_r/i_a

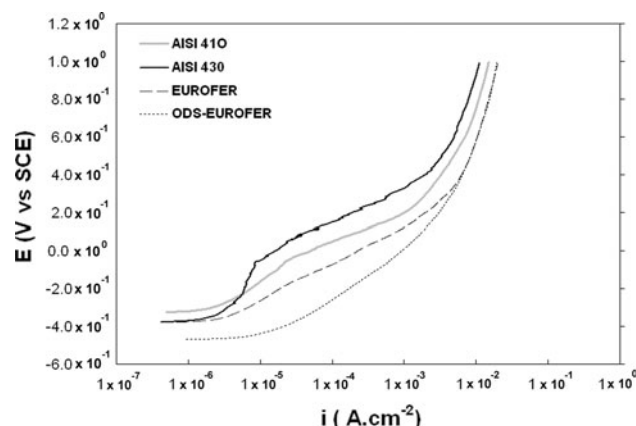


Fig. 4 Potentiodynamic polarization curves after 5 min of immersion in a 0.1 NaCl mol L⁻¹ solution at 25 °C

values obtained from the DL-EPR curves for the samples tested.

The results of Table 3 confirm that the ferritic AISI 430 stainless steel has the highest intergranular corrosion resistance, being approximately 9,000 times higher than the RAFM ODS-Eurofer alloy, which presented the highest susceptibility to intergranular corrosion. The i_r/i_a values also show that the intergranular corrosion resistance of RAFM Eurofer 97 alloy is approximately 1.2 times higher than the RAFM ODS-Eurofer alloy.

Micrographs of the samples after DL-EPR tests are shown in Figs. 6, 7, 8 and 9. These micrographs indicate a slight attack at the grain boundaries of ferritic AISI 430 stainless steel sample (Fig. 6); but on the other samples, not only the grain boundary regions are intensely corroded but noticeable corrosion has also occurred inside the grains of the tested samples (Figs. 7, 8, 9).

Severe attack of martensitic AISI 410 stainless steel samples, either inside the grains or at the grain boundaries, resulted in large material loss from these areas (Fig. 7). Consequently, despite the lower i_r/i_a value given in Table 3, this result cannot be correlated to its intergranular corrosion resistance.

Table 2 Values of resistance and CPE obtained for the AISI 430, AISI 410, Eurofer and ODS-Eurofer alloys in a 0.1 NaCl mol L⁻¹ solution at 25 °C, by fitting experimental data to the equivalent circuit of Fig. 2

	ODS- Eurofer	Eurofer 97	AISI 410	AISI 430
R _{sol} (Ω.cm ²)	89.18	66.51	74.18	81.31
R ₁ (Ω.cm ²)	5.55 × 10 ⁴	5.71 × 10 ⁴	8.28 × 10 ⁴	8.98 × 10 ⁴
CPE ₁ (cm ⁻² s ⁻ⁿ Ω)	8.26 × 10 ⁻⁵	5.04 × 10 ⁻⁵	5.85 × 10 ⁻⁵	5.30 × 10 ⁻⁵
n ₁	0.77	0.63	0.83	0.79
R ₂ (Ω.cm ²)	8.03 × 10 ⁴	17.28 × 10 ⁴	27.27 × 10 ⁴	67.93 × 10 ⁴
CPE ₂ (cm ⁻² s ⁻ⁿ Ω)	2.60 × 10 ⁻⁴	4.46 × 10 ⁻⁵	5.30 × 10 ⁻⁵	2.99 × 10 ⁻⁶
n ₂	0.45	0.87	0.53	0.99
χ ²	2.52 × 10 ⁻⁴	5.71 × 10 ⁻⁴	5.27 × 10 ⁻⁴	3.64 × 10 ⁻⁴

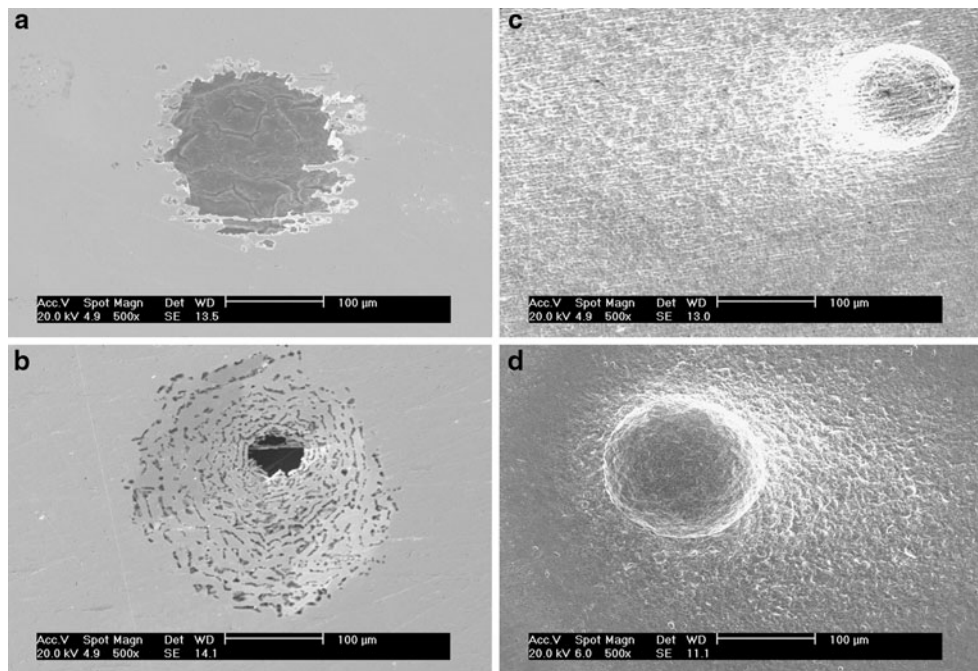


Fig. 5 Micrographs of the **a** AISI 430, **b** AISI 410, **c** Eurofer 97 and **d** ODS-Eurofer after potentiodynamic polarization tests in a 0.1 NaCl mol L⁻¹ solution, at 25 °C. Scanning electron microscopy

Table 3 i_r/i_a values estimated from DL-EPR test in 2 M H₂SO₄ + 0.005 M KSCN solution

Material	i_r/i_a
AISI 430	0.00002
AISI 410	0.00010
Eurofer 97	0.14600
ODS-Eurofer	0.17190

Figure 8 presents the high amount of inclusions on the surface of the RAFM Eurofer 97 alloy. These micrographs corroborate the study where round and elongated inclusions in some areas of this material were observed [3]. Nevertheless, most of these inclusions seems to be arranged in line, disagreeing with the literature [3], as they are not randomly distributed, but predominantly located at the grain boundaries (Fig. 8b).

It is clearly seen in Fig. 9 that RAFM ODS-Eurofer alloy has much more inclusions than RAFM Eurofer 97 alloy. Besides, Fig. 6a shows that, in this case, these inclusions are randomly distributed.

Figures 8, 9 and 10 indicate that the corrosion process of RAFM Eurofer alloy occurs in the vicinity of the precipitates, suggesting that these areas were the most susceptible to corrosion. Consequently, despite the i_r/i_a values shown in Table 3, it was not possible to correlate these values to

the intergranular corrosion resistance neither in Eurofer 97 steel nor in the ODS-Eurofer steel.

4 Conclusions

The ODS-Eurofer presented lower corrosion resistance than Eurofer 97 alloy. This difference becomes even larger when compared to AISI 410 and 430 stainless steels. The main difference between the chemical compositions of both Eurofer alloys studied in this work is the presence of Y, indicating that the addition of Y₂O₃ did not improve the corrosion resistance of ODS-Eurofer alloy.

The potentiodynamic polarization curves also confirmed that the Y₂O₃ in the RAFM ODS-Eurofer did not improve its corrosion resistance in comparison with RAFM Eurofer 97 alloy. The DL-EPR test could not evaluate the intergranular corrosion resistance of both Eurofer 97 and ODS-Eurofer alloys, since heavy corrosive processes occurred inside their grains, mainly in the vicinity of the precipitates. The SEM micrographs taken after DL-EPR tests proved that the RAFM ODS-Eurofer presents lower corrosion resistance than the RAFM Eurofer 97 alloy due to the larger amount of precipitates in the latter. The micrographs also show that both RAFM Eurofer 97 and ODS-Eurofer alloys have too many precipitates, which cause a decrease in their corrosion resistance. These particles are mostly located at the grain boundaries in the RAFM

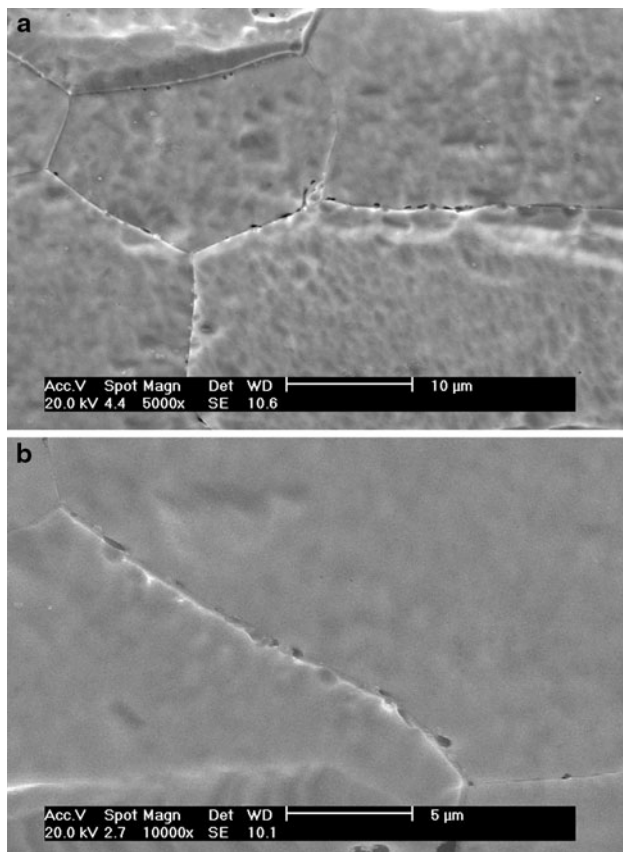


Fig. 6 SEM micrographs of ferritic AISI 430 stainless steel. **a** Intergranular corrosion and **b** detail of a grain boundary at a higher magnification. The micrographs were obtained after DL-EPR test in 2 M H₂SO₄ + 0.005 M KSCN solution at 25 °C

Eurofer 97 whereas in the RAFM ODS-Eurofer alloy they are found randomly distributed.

All electrochemical tests adopted in the present study, EIS, potentiodynamic polarization curves and DL-EPR diagrams, proved that ferritic AISI 430 stainless steel with the highest chromium content among the studied steels was also the stainless steel with the highest intergranular

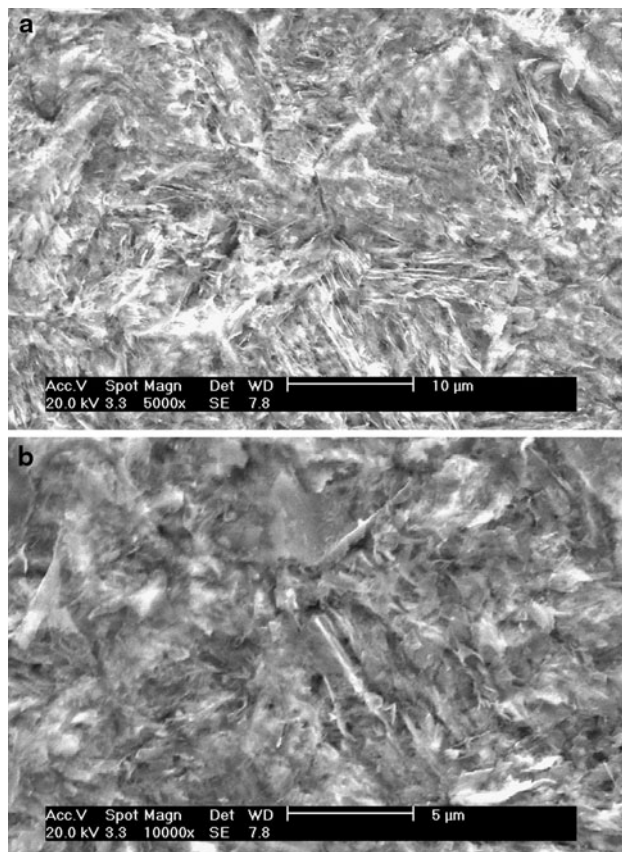


Fig. 7 SEM micrographs of martensitic AISI 410 stainless steel. **a** Severe attack at grain boundaries and inside the grains and **b** same as (a) at a higher magnification. The micrographs were obtained after DL-EPR test in 2 M H₂SO₄ + 0.005 M KSCN solution at 25 °C

corrosion resistance, in contrast with the other materials studied. However, despite the low i_i/i_a value obtained for the martensitic AISI 410 stainless steel, the SEM micrographs reveal that the samples were severely corroded not only at the grain boundaries but also inside the grains, indicating that this value could not be solely related to the intergranular corrosion phenomenon.

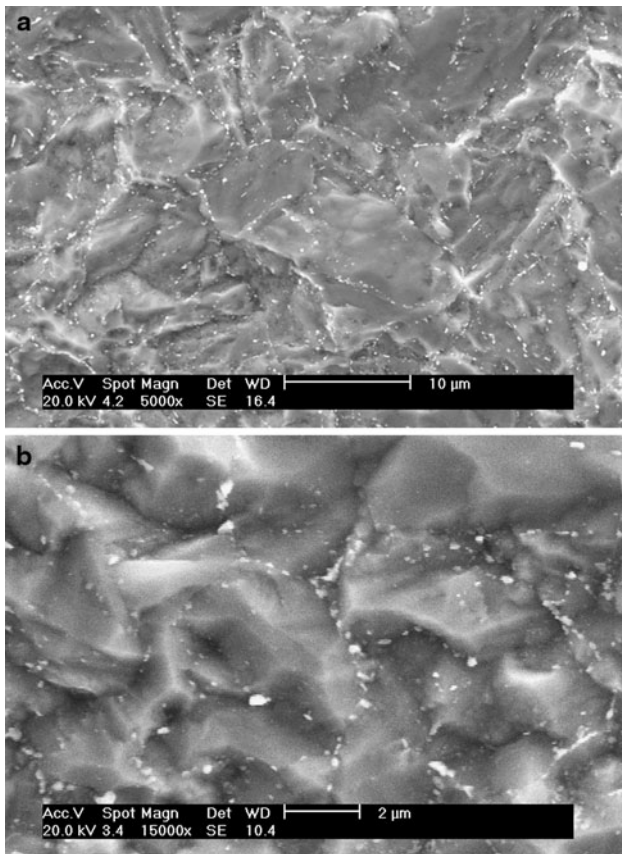


Fig. 8 SEM micrographs of RAFM Eurofer 97 alloy. **a** Corrosive attack at grain boundaries and inside the grains. A large number of precipitates can be visualized at the grain boundaries and **b** same as (a) at a higher magnification. The micrographs were obtained after DL-EPR test in 2 M H₂SO₄ + 0.005 M KSCN solution at 25 °C

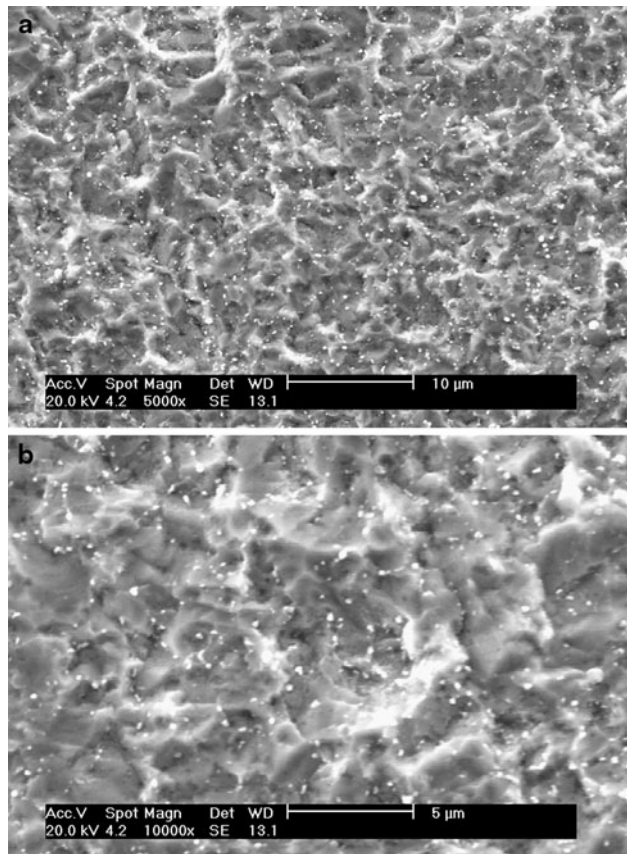


Fig. 9 SEM micrographs of RAFM ODS-Eurofer alloy **a** Generalized attack at the grain boundaries and inside the grains and **b** same as (a) at a higher magnification. The micrographs obtained after DL-EPR test in 2 M H₂SO₄ + 0.005 M KSCN solution at 25 °C

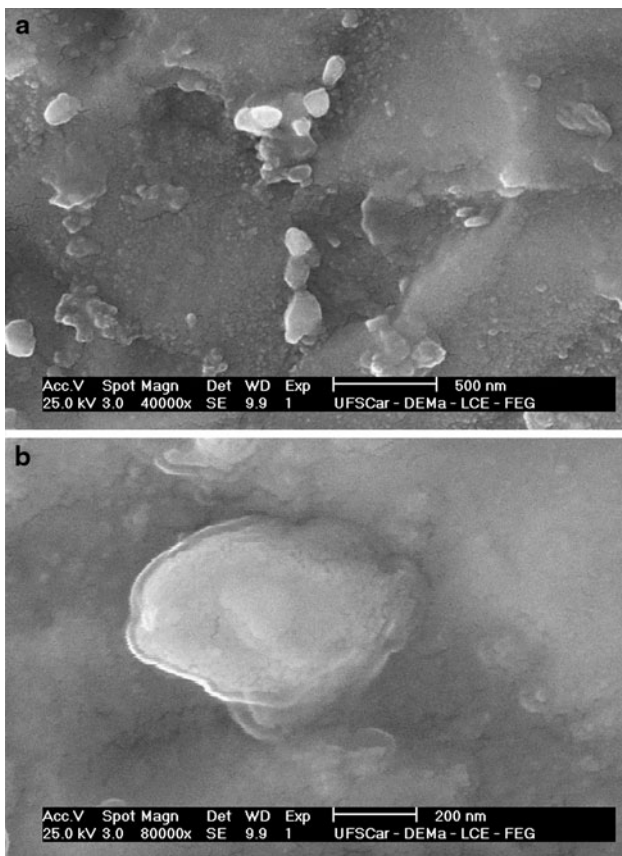


Fig. 10 Field emission gun SEM micrographs in RAMF ODS-Eurofer alloy after DL-EPR test in 2 M H₂SO₄ + 0.005 M KSCN solution at 25 °C. **a** Precipitates and **b** Detail of an individual particle at a higher magnification

Acknowledgments The authors acknowledge Fundação de Amparo à Pesquisa do Estado de São Paulo for the financial support (Grants 08/54836-4 and 07/56436-0) and to Dr. Anton Möslang and to Dr. Rainer Lindau (Forschungszentrum Karlsruhe, Germany) for kindly supplying the Eurofer samples. The authors also acknowledge Villares Metals for kindly supplying the AISI 410 and AISI 430 samples and the Universidade Federal de São Carlos for the field emission gun scanning electron microscopy analyses.

References

- Kohyama A, Hishinuma A, Gelles DS, Klueh RL, Dietz W, Ehrlich K (1996) J Nucl Mater 233:138
- Saito J, Suda T, Yamashita S (1998) J Nucl Mater 258:1264
- Fernández P, Lancha AM, Lapeña J, Hernández-Mayoral M (2001) Fusion Eng Des 58:787
- Kimura A, Kasada R, Kohyama A, Tanigawa H, Hirose T, Shiba K, Jitsukawa S, Ohtsuka S, Ukai S, Sokolov MA, Klueh RL, Yamamoto T, Odette GR (2007) J Nucl Mater 367:60
- Eiselt ChCh, Klimenkov M, Lindau R, Möslang A, Sandim HRZ, Padilha AF, Raabe D (2009) J Nucl Mater 385:231
- Coppola R, Lindau R, May RP, Möslang A, Valli M (2009) J Nucl Mater 386–388:195
- Hadraha H, Dlouhy I (2009) J Nucl Mater 386–388:564
- Klimentov M, Lindau R, Möslang A (2009) J Nucl Mater 386–388:557
- Lu Z, Faulkner RG, Riddle N, Martino FD, Yang K (2009) J Nucl Mater 386–388:445
- Olier P, Bougault A, Alamo A, de Carlan Y (2009) J Nucl Mater 386–388:561
- Heintze C, Bergner F, Ulbricht A, Hernández-Mayoral M, Keiderling U, Lindau R, Weissgärtner T (2010) J Nucl Mater (in press)
- Li M, Zhou Z, He P, Liao L, Xu Y, Ge C (2010) Fusion Eng Des 85:1573
- Sandim HRZ, Renzetti RA, Padilha AF, Raabe D, Klimentov M, Lindau R, Möslang A (2010) Mater Sci Eng A 527:3602
- Williams CA, Marquis EA, Cerezo A, Smith GDW (2010) J Nucl Mater 400:37
- Yamamoto M, Ukaia S, Hayashi S, Kaito T, Ohtsuka S (2010) Mater Sci Eng A 527:4418
- Aleev AA, Iskandarov NA, Klimentov M, Lindau R, Möslang A, Nikitin AA, Rogozhkin SV, Vladimirov P, Zaluzhny AG (2011) J Nucl Mater 409:65
- Fernández P, Eddahbi M, Auger MA, Leguey T, Monge MA, Pareja R (2011) J Nucl Mater (in press)
- Eiselt ChCh, Klimentov M, Lindau R, Möslang A (2011) J Nucl Mater (in press)
- Dapeng Z, Yong L, Feng L, Yuren W, Liuji Z, Yuhai D (2011) Mater Lett 65:1672
- Li Y, Nagasaka T, Muroga T, Kimura A, Ukai S (2011) Fusion Eng Des (in press)
- Klueh RL, Harries DR (2001) High-Chromium ferritic and martensitic steels for nuclear applications. ASTM, New Jersey, USA
- De Castro V, Leguey T, Muñoz A, Monge MA, Fernández P, Lancha AM, Pareja R (2007) J Nucl Mater 367:196
- Klimiankou M, Lindau R, Möslang A (2007) J Nucl Mater 367:173
- Benamati G, Fazio C, Ricapito I (2002) J Nucl Mater 307–311:1391
- Aiello A, Agostini M, Benamati G, Long B, Scaddozzo G (2004) J Nucl Mater 335:217
- Konys J, Krauss W, Voss Z, Wedemeyer O (1379) J Nucl Mater 2004:329–333
- Splíchal K, Zmitko M (1384) J Nucl Mater 2004:329–333
- Konys J, Krauss W, Voss Z, Wedemeyer O (1144) J Nucl Mater 2007:367–370
- Moreau R, Bréchet Y, Maniguet L (2011) Fusion Eng Des 86:106
- Vankeerberghen M, Bosch R-W, Van Nieuwenhoven R (2003) J Nucl Mater 312:191
- Van Dyck S, Bosch R-W (2005) Fusion Eng. Des. 75–79:973
- Lee JB (1981) Corrosion 37:437
- Lee JB (1986) Corrosion 42:106
- Padilha AF, Plaut RL, Rios PR (2007) In: Steel heat treatment handbook, 2nd ed. CRC Press, FL, USA
- Zingales A, Quartarone G, Moretti G (1985) Corrosion 41:136
- Terada M, Saiki M, Costa I, Padilha AF (2006) J Nucl Mater 358:40
- ASTM A262-10 Standard Practices for Detecting Susceptibility to Intergranular Attack in Austenitic Stainless Steels